Document downloaded from:

http://hdl.handle.net/10251/183015

This paper must be cited as:

Pastor, JV.; García Martínez, A.; Mico Reche, C.; De Vargas Lewiski, F.; Vassallo, A.; Pesce, FC. (2021). Effect of a novel piston geometry on the combustion process of a light-duty compression ignition engine: An optical analysis. Energy. 221:1-11. https://doi.org/10.1016/j.energy.2021.119764

The final publication is available at

https://doi.org/10.1016/j.energy.2021.119764

Copyright Elsevier

Additional Information

Effect of a novel piston geometry on the combustion process of a light-duty compression ignition engine: an optical analysis

José V. Pastor[a], Antonio García[a], Carlos Micó[a], Felipe Lewiski[a], Alberto Vassallo[b], Francesco Concetto Pesce[b]

[a]CMT - Motores Térmicos, Universitat Politècnica de València, Camino de Vera s/n, 46022 Valencia, Spain

[b]PUNCH Torino S.p.A, Corso Castelfidardo, 36, 10129 Torino TO, Itália

Corresponding author (*): Carlos Micó

e-mail: carmirec@mot.upv.es

Phone: +34 654919619

Abstract

The development of new piston geometries has shown great potential to achieve the low levels of soot emissions required by regulation. Thus, the present paper aims to characterize the influence of a new piston design over combustion process. It is characterized by the introduction of protrusions around the periphery of the bowl, evenly spaced. The performance of this geometry is compared to other geometries that have been extensively analyzed in literature, under similar operating conditions. To achieve this objective, a single cylinder optical compression ignition engine was used with full-quartz pistons representing three bowl geometries: re-entrant, stepped lip and wave-stepped lip. Two optical techniques (OH* chemiluminescence and Natural Luminosity-NL) were applied for identifying the near-stoichiometric zones and the differences in the combustion evolution. The flame movement was analyzed by applying the combustion image velocimetry (CIV) algorithms. In addition, an in-cylinder pressure analysis was performed for each piston at 4.5 bar and 7.5 bar IMEP and the differences in terms of Rate of Heat Release were highlighted. A more intense reverse flow was clearly identified when using wave protrusions inside the bowl. The stepped lip and

wave-stepped lip bowl present faster late cycle oxidation with much near-stoichiometric zones than re-entrant piston.

Keywords

Optical engines; Optical Techniques; bowl geometry; compression ignition; combustion image velocimetry.

1. Introduction

The reduction of pollutant emissions from internal combustion engines (ICE) in order to cover all emissions legislations is currently one of the most important challenges for the automotive industry and engine researchers. Regarding diesel combustion, emissions reduction is even a more complex problem due to the existence of the well-known soot and NOx trade-off. However, different ways have been studied and applied to improve the engine thermal efficiency and reduce soot emissions. Numerous works can be found in the literature where researchers have focused on the application of new combustion strategies or alternative fuels in compression ignition (CI) engines. On one hand, new concepts like RCCI[1][2][3][4] and PPC [5][6]. On the other hand, the use of alternative fuels such as biodiesel [7][8][9] and synthetic fuels [10][11][12][13] in conventional CI operating conditions. A different approach for pollutant reduction and emission improvement is the implementation of new hardware concepts. In this regard, great attention has been paid during the last years to the development of new piston geometries[14].

The in-cylinder soot formation and oxidation can be related with the air/fuel mixture formation process. It is affected mainly by the injection system, piston geometry and fuel properties. All of them have the purpose of promoting an efficient fuel-air mixing

and combustion processes. However, a better mixing process usually leads to a higher flame temperature and consequently a significant increase in NO_X formation. For this reason, recent works have focused on promoting soot oxidation during late combustion stage [15][16]. At this point, the piston geometry takes a major role as it influences both swirl and squish flows and spray-walls interaction, as well as the late-cycle mixing process [17][18][19].

Different studies have been developed in order to understand flame movement inside the piston bowl and its interaction with the walls [20][21][22][23]. For light and medium-duty diesel engines, where the swirl number is usually higher than 1, the piston bowl design is typically re-entrant, as shown in figure 1. The purpose of this geometry is to support the swirl movement generated inside the cylinder, creating a re-circulation flow towards the bowl center during the late combustion stage [15].

Different re-entrant geometries have been developed and optimized during the last years. A milestone in this regard was the inclusion of a chamfered or stepped lip (figure 1) in replacement of the protruding lip which is usual in re-entrant geometries. Several companies have explored its potential. Nelly et al. [24] tested a 2.2 L 4-cylinder diesel engine using a stepped lip bowl geometry developed by Honda. Ricardo UK company developed, patented [25] and tested [26] in 2011 a piston geometry where the bowl includes a stepped lip design. All these works reported significant soot reduction due to the better fuel-air mixing. Additionally, the combustion duration with the stepped lip geometry is shorter than the re-entrant one [18][27], which impacts in a thermal efficiency improvement and a consequent fuel consumption reduction[26].

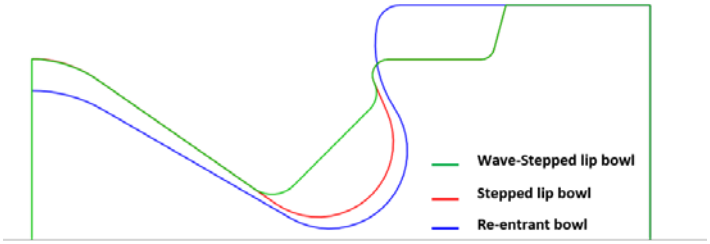

Figure 1- Sketch of the different bowl geometries

Recently, Volvo Group [28] presented its new piston named "wave piston" which was developed for truck engines. The piston is formed by wave protrusions distributed around the circumference of the outer bowl. Some previous works [15][19] reported a decrease of up to 80% in soot emissions and a strong reduction of soot vs NO_X trade-off. In addition, a reduction of the fuel consumption could be appreciated as well.

The benefits of the wave-protrusions have been demonstrated for heavy-duty engines. However, this concept has been never applied in light-duty engines. For these small engines, the higher swirl ratio and the strong flow movement could result in different flame-air flow interaction. Considering this, the current paper aims to fill this gap by studying the performance of wave-protrusions in a light-duty engine. Therefore, the objectives of this work are: first, to analyze the effect of a new bowl geometry, which includes wave-protrusions, on the flame movement along the combustion cycle; second, to characterize the influence of the new bowl geometry on combustion performance. The new concept mixes the stepped-lip and wave-protrusion geometries (figure 1), with the aim of combining the benefits of both proposals in terms of soot reduction and thermal efficiency improvement. This novel piston geometry is compared with two already known geometries: stepped-lip and reentrant. For this purpose, a single cylinder optical CI engine with three different quartz piston bowl geometries (re-entrant, stepped lip and wave-stepped lip) was utilized. The in-cylinder pressure signal was used

to obtain the RoHR for each piston tested. In addition, two optical techniques were applied simultaneously in order to analyze the differences in the combustion process. The flame natural luminosity (NL) was registered and used to study its movement inside the combustion chamber by applying the combustion image velocimetry algorithms. In addition, OH* chemiluminescence was used for the identification of high temperature reaction zones where air/fuel ratio is close to the stoichiometric value. The novelty of this work is the description of the air and flame movement caused by the use of wave protrusions in a piston bowl of a light-duty engine. In addition, it is the first study where the wave-protrusion effect is analyzed in detail in an optical engine, considering both heavy-duty and light-duty application. The results shown in this paper can contribute for the optimization and development of more efficient and less pollutant CI engine pistons.

2. Experimental methodology

2.1. Optical CI engine

The tests were performed in an optical compression ignition engine (figure 2). The optical engine is based on a GM commercial engine which has a displacement of 400 cm^3 per cylinder. In addition, it is equipped with an original GM cylinder head with a centrally located Denso solenoid injector and 4 valves per cylinder. Stroke and bore are the same used in the GM metal engine. Table 1 summarizes the geometric parameters of the optical engine.

Table 1. Optical engine characteristics

Engine type	4 stroke, direct injection
Num. Valves [-]	4
Num. of cylinders [-]	1
Stroke [mm]	80.1
Bore [mm]	80
Bowl Types	Re-entrant /stepped lip/Wave-stepped lip
Compression ratio [-]	12.5:1 (re-entrant)/ (11.5:1 (hybrid)

Displacement [l]	0.402

The main optical access to the combustion chamber is achieved using a fully transparent quartz piston. In order to replicate the combustion process and flow dynamics present in a real metal engine, the different transparent pistons used included a bowl shape similar to the full-metal ones. The rings of the piston consist of a synthetic material developed for expanding with temperature increase.

The injection system uses a conventional fuel pump and common rail. The DRIVVEN® control unit controls the injector and allows the adjustment of different injection parameters.

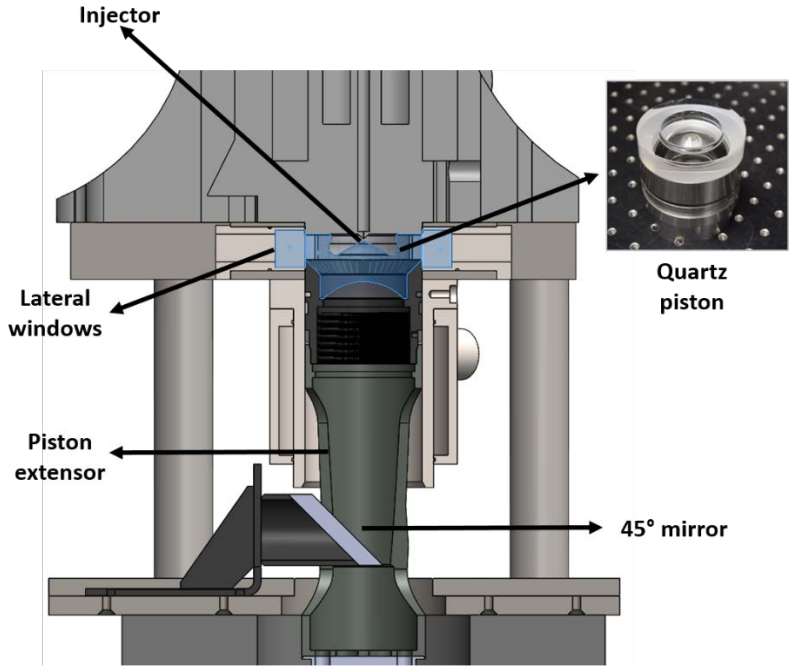

Figure 2- Optical Engine

2.2. Engine test cell

The figure 3 represents the equipment necessary to operate the engine, including data acquisition and control. A screw compressor supplies the intake air up to 30 bar of pressure and a maximum flow rate of 400 kg/h. The intake air is prepared by a heat

exchanger and a dryer. An air heater is located at the settling chamber and it ensures a constant intake air temperature. A backpressure regulator is installed in the exhaust system. To avoid pressure pulses in the intake and exhaust lines, settling chambers were used.

The engine load and speed are controlled by an electric dynamometer. The schenck electric dynamometer has a maximum power of 220 kW, a maximum torque of 562 nm and a maximum speed of 9000 rpm. The intake and exhaust pressure were measured with piezoresistive transductor (Kistler-4603B10). A piezoelectric transductor (AVL GH13P glow-plug) was used for the in-cylinder pressure measurement. A Yokogawa DL7008E oscilloscope recorded the instantaneous pressure signals. The acquisition system was synchronized by using a shaft encoder with a resolution of 0.2 CAD. The accuracy of the devices is shown in Table 2.

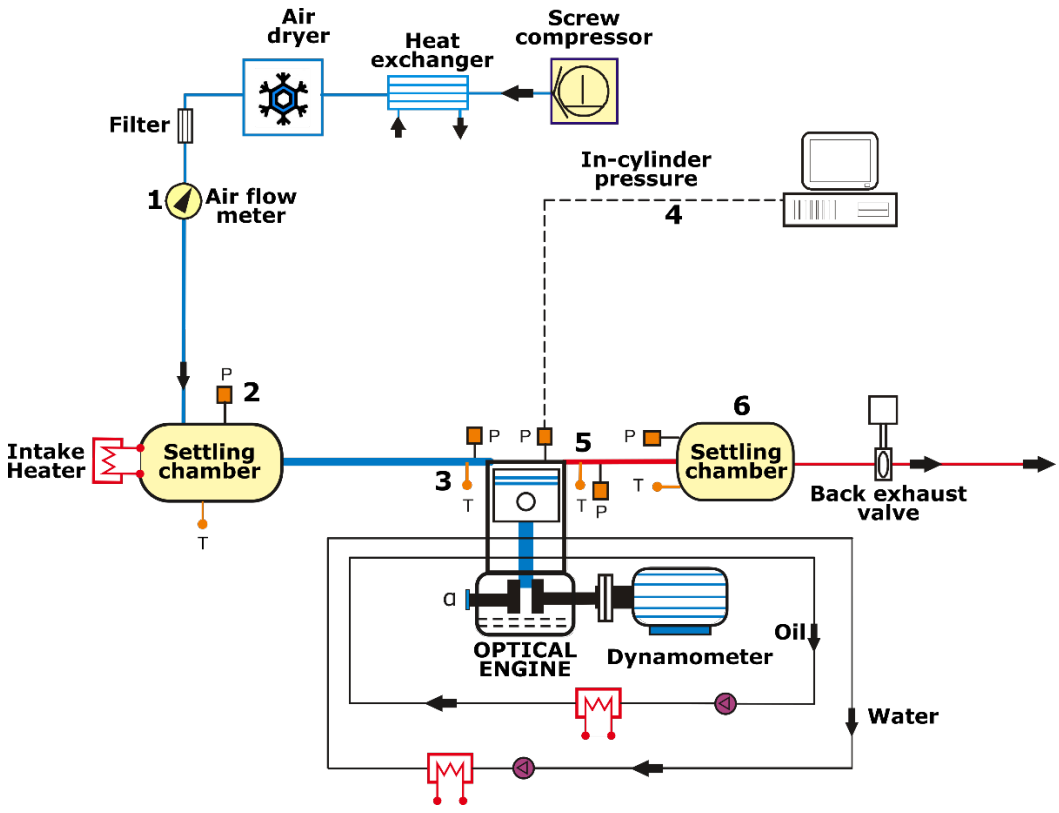

Figure 3 – Test cell diagram

Table 2 – Accuracy of the sensors

Location	Variable	Device	Manufacturer / model	Accuracy
3-5	Intake/exhaust pressure	Piezorresistive transducers	Kistler / 4603B10	±25 mbar
4	In-cylinder pressure	Piezoelectric transducer	AVL / GH13P	±1.25 bar
	Engine speed, crank angle,	Encoder	AVL / 364	±0.02 CAD
1	Air mass flow	Air flow meter	Sensyflow / FTM700-P	< ±1%
2-6	Temperature in manifolds and settling chambers	Thermocouple	TC direct / type K	±2.5 °C

2.3. Bowl geometries

For the present work, three different bowl geometries were tested in the optical engine. A piston with reentrant geometry (figure 4a) was tested as the baseline. Besides, a kind of hybrid design combining two bowl geometries in the same piston was developed. One half of the piston, represented in figure 4b, was formed only by the stepped lip geometry. The other one was composed by the stepped lip and wave geometry. The main purpose of the hybrid piston was to compare performance of two bowl geometries in the same combustion cycle. The quartz pistons were manufactured by a German company.

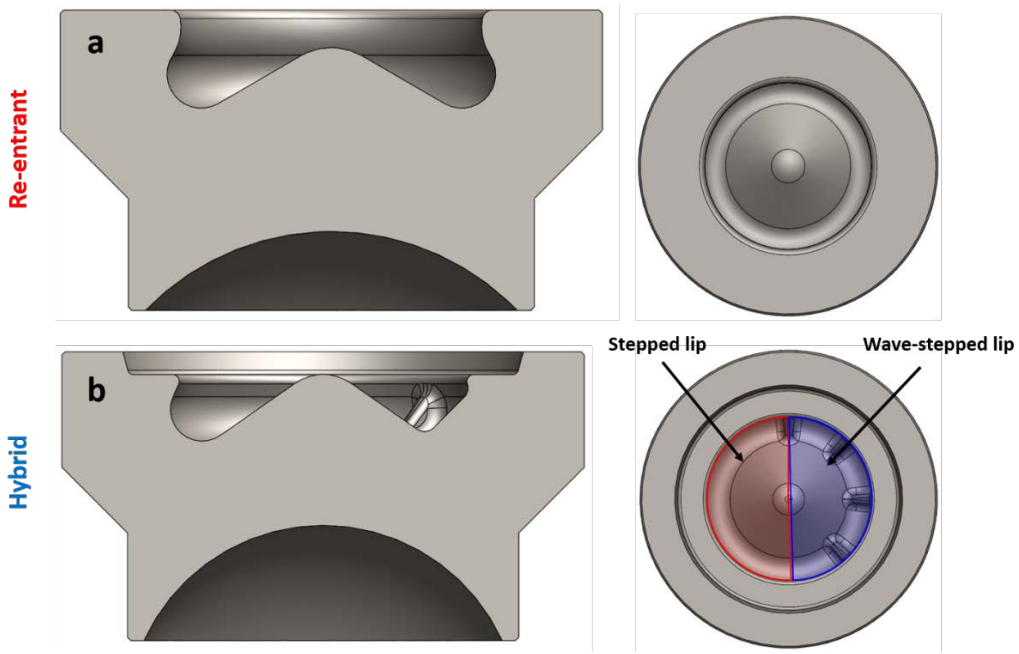

Figure 4 – Bowl geometries: a) Re-entrant. b) Hybrid

2.4. Operating conditions

Experiments were performed with commercial diesel fuel and two different engine loads: 4.5 and 7.5 bar of IMEP. For the two loads the engine speed was kept constant at 1250 rpm. Considering that the two pistons do not have the same compression ratio, different intake temperatures and intake pressures were set in order to maintain the same IMEP and mass of fuel injected per cycle as well as the same maximum in-cylinder pressure (P_{max}). In figure 5, the result of the in-cylinder thermodynamic adjustment between both pistons is shown. It was based on keeping similar in-cylinder pressure and density around TDC for motored cycles, which ensured the same in-cylinder conditions just before the pilot 1 ignition for the two pistons tested. Figure 5a represents the in-cylinder pressure and density for the condition of 7.5 bar IMEP and figure 5b the condition of 4.5 bar IMEP. Additionally, the test matrix is represented in table 3. An exhaust backpressure was used in order to mimic real engine conditions.

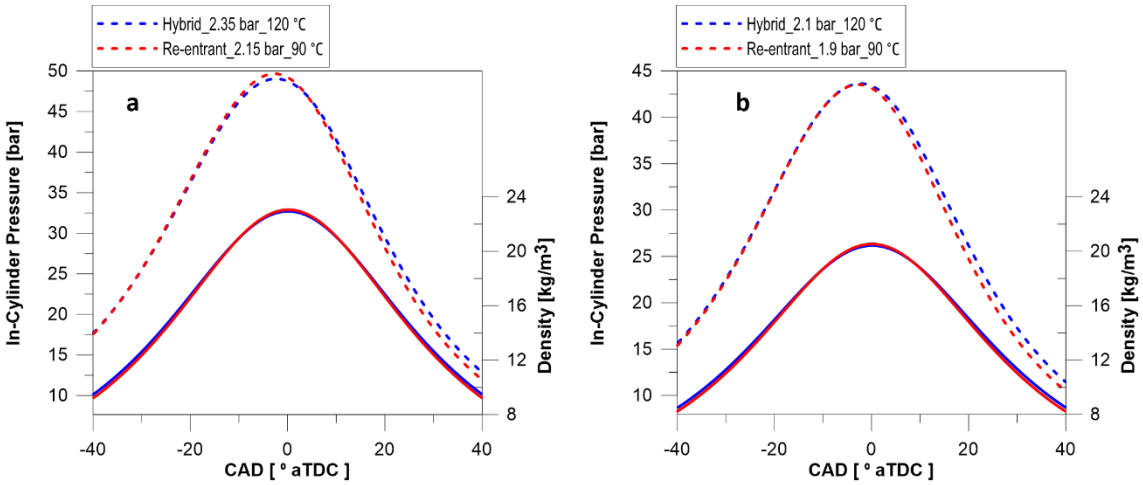

Figure 5 – a) motored In-cylinder pressure (dashed line) and density (continuous line) corresponding to 7.5 bar IMEP operating conditions. b) motored In-cylinder pressure (dashed line) and density (continuous line) corresponding to 4.5 bar IMEP operating conditions

Table 3- Engine operating conditions

Inj. Pattern	Engine Speed	Piston	IMEP (bar)	$\dot{m_{air}}$ (1) (g/s)	Pint(P_3) (Bar)	Tint(T_3) (°C)	Toil (°C)	Tcool (°C).
Mult.	1250	Re-entrant	4.5	7.26	1.9	90	60	15-25
		Hybrid		7.55	2.1	120		
		Re-entrant	7.5	8.08	2.15	90		
		Hybrid		8.5	2.35	120		

Four injections per cycle (pilot 1, pilot 2, main and post) were configured to mimic a commercial injection strategy. It was used different injection pressures (800 and 670 bar) for each IMEP tested. These injection settings were applied for both pistons.

2.5. Optical Techniques

For the present work, two optical techniques were applied for identifying the differences between each bowl geometry. The optical setup was designed in order to record the flame radiation trough the piston bottom. In figure 6, the optical assembly used for the tests is shown.

To measure OH* chemiluminescence, an intensified camera (ICCD) was positioned in parallel with the engine's crankshaft and the UV radiation was reflected by means of a dichroic mirror. Considering that the dichroic is transparent to the visible range (up to 750 nm), the NL camera was positioned 90 ° relative to the engine's crankshaft just behind of the dichroic mirror. A 45° elliptical mirror was positioned just below the piston in order to reflect all flame radiation from the combustion chamber towards the optical system.

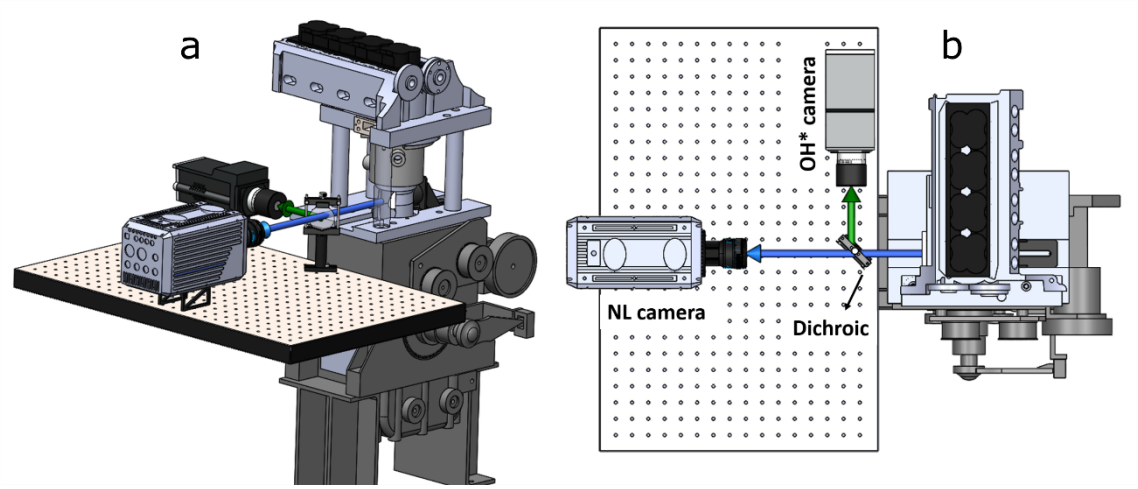

Figure 6 - Optical setup – a) Isometric view - b) Top view

2.5.1. High-Speed Natural Luminosity Imaging

The Natural luminosity (NL) signal corresponds to the thermal soot radiation emitted during the combustion process. It allows to analyze the effect of each piston geometry in terms of combustion evolution and flame structure. Images were registered from the start of energizing of the first pilot injection until the end of combustion. A Photron SA-5 high speed CMOS camera with an exposure time of 6.65 µs and a frame rate of 25 kFPS was used to record the images. A Carl Zeiss Makro-Planar T 100mm f/2 ZF2 camera lens was mounted in the camera. The image resolution was 512 x 512 pixels with a spatial resolution of 8.1 pixels/mm.

2.5.2. OH* chemiluminescence

Spontaneous radiation emitted by the excited-state OH* molecules was used to visualize the near-stoichiometric high temperature zones, where combustion is taking place and soot oxidation is promoted. An Andor Solis iStar DH334T-18H-83 intensified camera was used. The spatial resolution of the image was 8.75 pixel/mm. In addition, a Bernhard-Halle UV lens, with 100 mm focal length and f/2, and a 310 nm ± 10 nm bandpass filter were mounted in the camera. Considering that the maximum framerate of the camera allows one image per cycle, a sweep of 6 different CAD was performed.

2.6. Combustion Image Velocimetry - CIV

Combustion image velocimetry (CIV) is a technique similar to Particle Image Velocimetry (PIV) but, in this case, the tracking source is the light emitted by the soot particles [17]. It is a very useful technique, especially when applying standard PIV is not possible. The use of complex bowl geometries, as it was in this work, causes both the refraction of the laser source and the distortion of the images. CIV technique has been applied in different studies in order to obtain semi-quantitative information about velocity fields and flow patterns inside the bowl under reactive conditions[17][29].

In this work, CIV was used with NL images, where most of the signal corresponds to soot radiation. A cross-correlation algorithm was applied to pairs of consecutive NL images to calculate instantaneous velocity fields. However, quantification of CIV-resolved velocity is very difficult. Soot particle clouds are three-dimensional objects, and light received by the detector is the integration of the whole cloud. Thus, observed movement is not located at a specific measuring plane and flame tracking is sometimes difficult. Nonetheless, this technique is still valuable to provide semi-quantitative results

of the in-cylinder flow. For this paper, CIV has been used to provide qualitative information of the flow pattern for each piston geometry based on the analysis of the flame movement. Calculations were performed with PIVlab [30] software. The interrogation window was varied from 80x80 pixels to 40x40 pixels with a time between each frame of 40 μs.

2.7. In-cylinder pressure analysis

The in-cylinder pressure measurements were used to calculate the rate of heat release (RoHR) and other combustion characteristic parameters. The RoHR curve was calculated by means of an in-house developed tool [31][32] which is based on first law of thermodynamics. The analysis is applied to a one zone model during the time that both exhaust and intake valves are closed. In addition, the model considers for its calculation the heat transfer, blow-by and mechanical deformations. An specific characterization was developed for this optical engine [33], which has been used also in this work. Combustion parameters such as combustion duration, combustion phasing (CA50) and start of combustion can be obtained from the same analysis.

3. Results and discussion

The current section first addresses the piston geometry influence through a thermodynamic analysis of the combustion process. After that, their influence on flame movement and flow pattern are discussed, based on NL images and the CIV results. Finally, combustion evolution for each geometry is described thanks to a combination of NL and OH* chemiluminescence images.

3.1. Thermodynamic analysis

A thermodynamic analysis only allows to compare both pistons, as it was not possible to isolate the effect of each side of the hybrid piston's bowl. In figures 7 and 8, the in-cylinder pressure and Rate of Heat Release (RoHR) are presented for the two pistons tested, at two different operating conditions: 7.5 and 4.5 bar IMEP respectively. A good agreement between the in-cylinder pressure (maximum value and evolution) of both piston geometries was achieved, as it can be seen in figures 7 and 8. At 7.5 bar IMEP, the four injections are clearly observable in the RoHR diagram and some differences can be highlighted between pistons. The fuel injected during the pilot 1 seems to burn faster for the hybrid piston than for the re-entrant piston, as the rate of energy released during this stage is higher. As the engine load is reduced, the differences between the pistons reduces as well. At low load (4.5 bar IMEP), the fuel-air ratio is around 35% lower than for 7.5 bar IMEP. It means that, under this operating condition, more oxygen is available. This reduces the contribution of the improved air-fuel mixing process associated to the hybrid geometry when it is compared with the re-entrant one. In addition, in the end of the pilot 2 the same behavior can be appreciated. Hybrid piston seems to burn fuel faster as the heat release rate suggest complete combustion. In this case, the RoHR decreases almost to 0 J/° before the main injection starts. During the main injection, the maximum RoHR peak is slightly higher for the hybrid piston, indicating faster mixing. In addition, the hybrid piston presents lower RoHR peak during the post injection, indicating less residual of non-burned fuel during the main injection combustion. For both engine loads, a shorter late-stage combustion (greyed area) after the post injection can be observed for the hybrid piston in comparison with the re-entrant one. The RoHR diagram at this stage decreases faster for the first case, indicating a shorter combustion

duration. This could be related with a better oxygen utilization inside the cylinder[34]. Taking into account that the stepped lip is present in both sides of the hybrid piston, these results agree with previous studies [17][35][27][18] using similar stepped lip geometries, where the authors have reported a faster late-cycle heat release decrease and a higher heat release rate (maximum peak) during the main part of the diffusion combustion. These previous results corroborate with the RoHR shown in the figures 7 and 8.

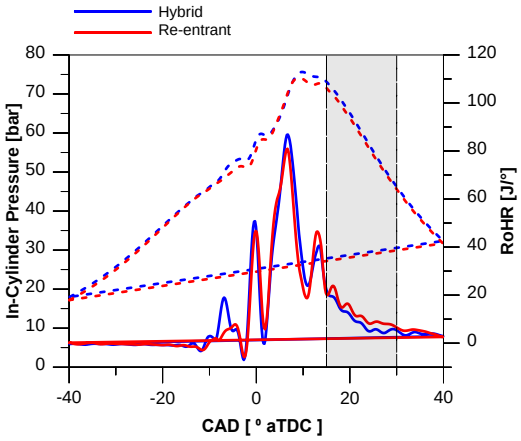

Figure 7- In-cylinder pressure and RoHR at 7.5 bar IMEP

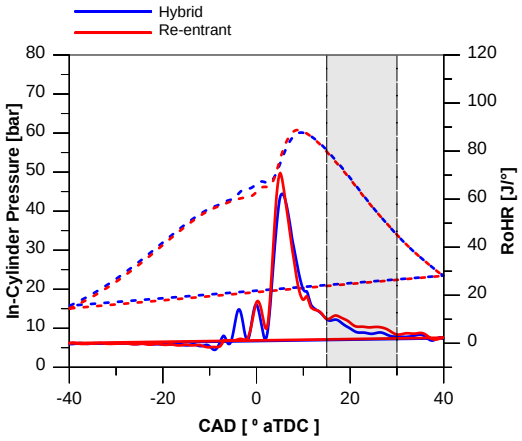

Figure 8- In-cylinder pressure and RoHR at 4.5 bar IMEP

3.2. Flame movement and flow patterns

Details regarding flame movement and flow patterns are reported in figure 9 and 11 for 7.5 bar IMEP. In both figures, the left side represents the re-entrant piston while the right side represents the hybrid piston. As it has been described previously, this one includes the others two bowl geometries: stepped lip without waves (left side) and wave-stepped lip (right side). At 7.7 CAD, in figure 9, main injection is occurring, and the spray is interacting with the bowl wall. The yellow lines represent the wave protrusions position in the piston. In addition, the red arrows represent the flame movement during the flame-wall interaction. At this instant, major differences can be detected when

comparing the side with waves with the other two geometries. When the sprays collide with the bowl wall, the wave protrusions avoid the flame to spread tangentially and redirects it toward the bowl center (red line area), minimizing the flame-flame collisions, providing a pathway for the oxygen supply to flame front and generating less fuel rich zones. This improves the oxidation of soot pockets [19]. In contrast, without waves, flame-flame collisions are observable close to the bowl wall. In this region the fuel/air ratio is much higher as the fresh ambient gas cannot reach these fuel rich zones[15]. During flame-flame interaction, products of combustion are mixed and the turbulent kinetic energy available in the jets is lost because of the collision. Thus, it leads to a creation of stagnation zones inside the bowl where low amount of oxygen is available.

Focusing on the hybrid piston, at 11.9 CAD (end of main injection) different flame structures can be seen for each piston geometry. The red line represents the area reached by the flame inside the bowl with waves while the orange line represents the area occupied by the flame at the side without waves. When both are compared, it is possible to see that the orange area is much smaller than the red one. Therefore, it can be stated that the flame in the stepped lip side without waves seems to remain concentrated at the periphery of the bowl. This behavior has been related with effect of the stepped lip, splitting the spray/flame into two parts (one inside the bowl and the other into the squish area) and reducing the momentum of the spray. Besides, the flame-flame collisions when not using wave protrusions and the resulting stagnations have been considered also a potential cause. In the case of the wave-stepped lip, the reverse flow forces the flame to move towards the bowl center. For the re-entrant geometry, even though the flame goes toward the center due to higher spray momentum, the existence of strong flame-wall and flame-flame interaction can

promote the formation of fuel rich zones. The same behavior for the wave protrusions was reported by Eismark et al.[19][15], where the stagnation zone formed during the flame-flame collision is smaller for the wave piston in comparison with a conventional one.

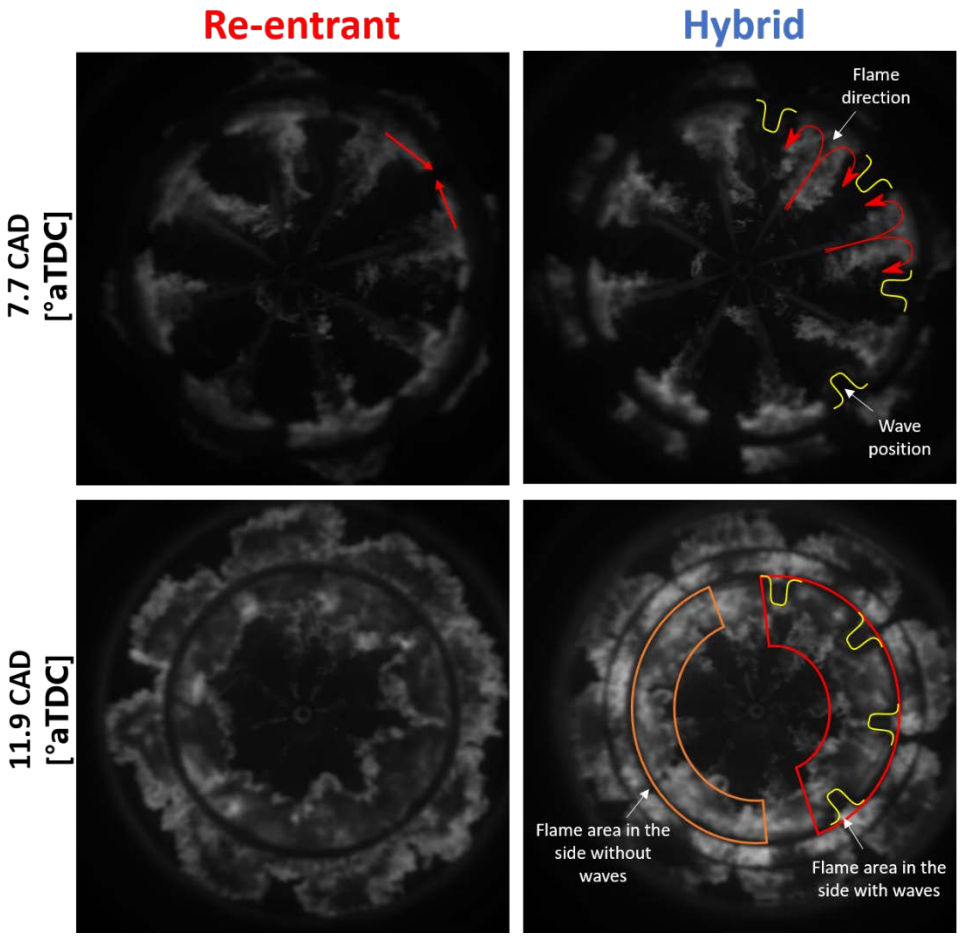

Figure 9- Flame behavior for the different bowl templates at 7.5 bar IMEP

This behavior is confirmed when the CIV velocity fields are analyzed (figure 11). In order to clarify the correspondence of the images include in the manuscript, figure 10 represents the injection mass flow rate. Additionally, the CADs corresponding to the CIV

velocity maps shown in figure 11 have been also represented. For the hybrid piston, at the wave-stepped lip side, it is possible to see the effect of the waves on the flame movement. A characteristic reverse flow is observed according to the vectors' direction, as it has been already discussed. Thus, the zones with fresh oxygen at the center of the bowl can be reached by the flames. In contrast, the side without waves presents lower velocities and the vectors are not directed towards the bowl center. When comparing with the re-entrant bowl, a similar reverse flow to the one described before can be observed. The velocity field is more intense than for the hybrid piston. In this case, the spray is not split in two parts and all kinetic energy is concentrated inside the bowl. At 9.5 CAD, it is possible to see that the re-entrant piston presents higher outward velocities in the squish region than the hybrid piston. In addition, the inward velocities are also weaker for this piston. This effect could be linked with the higher swirl amplification for the re-entrant piston as already reported and explained by Zha et al. (2018). Another difference that can be observe when comparing re-entrant and wave-stepped lip geometries is that, in the first case, an tangential flame movement inside the bowl is occurring. This is not observable in the hybrid piston, probably due to the presence of the wave protrusions and the reduction of the spray momentum inside the bowl.

For each CAD represented in figure 11 together the velocity field, the velocity profile corresponding to a line crossing the center of each piston is shown. This is represented by a green line drawn in the piston sketch. Looking at the plots, the velocity profile shows that the side with wave protrusions promotes higher velocities inside the bowl than the other side, without waves. In contrast, the velocity profile for the re-entrant piston seems to be very symmetric. At 11 CAD, the behavior of each piston is different. The re-

entrant piston presents high flame velocity but the flow of the hybrid piston starts to slow down, even though the wave side still shows slightly higher velocity values. At 17 CAD, just after the post injection, the re-entrant piston has a global reduction in the velocity and the vectors indicate that the flow seems to be driven only by the swirl motion. In the hybrid piston, the post injection accelerates the flow toward the periphery and the velocity field shows a small increment. For this piston, the typical swirl movement cannot be perceived as intense as for the re-entrant piston (especially in the wave protrusion side).

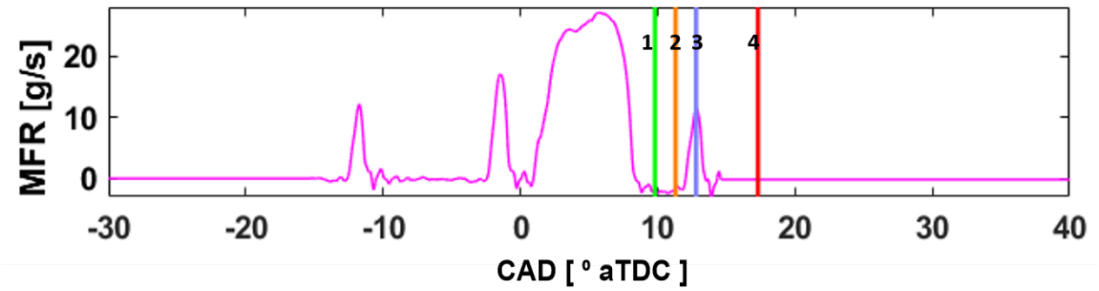

Figure 10- Mass flow rate of injection for the CIV measurements

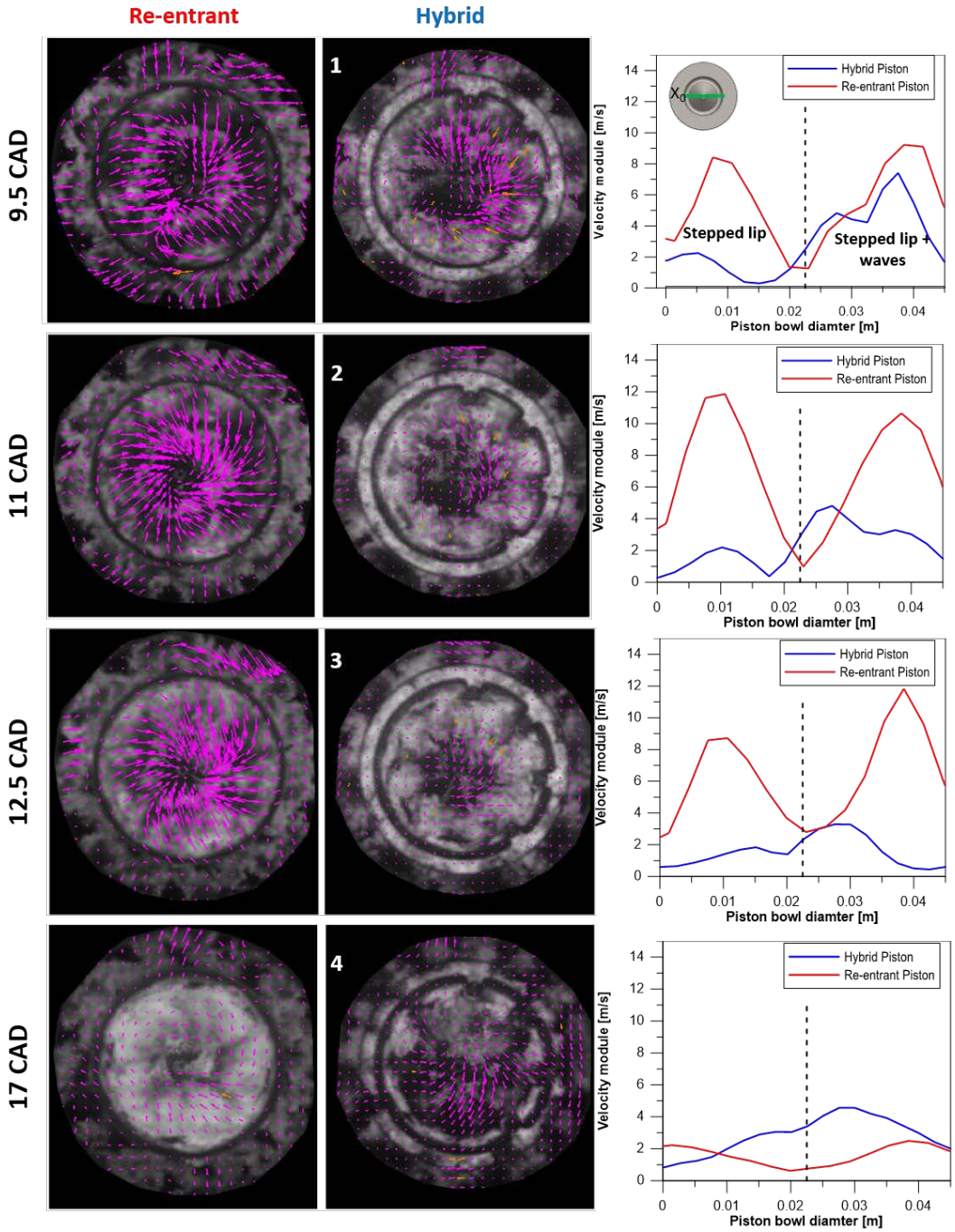

Figure 11- Velocity field analysis for different CADs

3.3. Combustion evolution

The combustion evolution for each geometry, at 7.5 bar IMEP, is represented in figure 13 by means of NL and OH* chemiluminescence images. For clarification, the mass flow rate has been included again in figure 12, indicating the CAD corresponding to the images shown. Starting at -4.15 CAD, early OH* chemiluminescence can be seen after

the pilot 1 injection. The OH* intensity seems to be slightly higher for the hybrid piston and more distributed inside the bowl, corroborating with the RoHR curve presented previously that more intense reactions are taking place at this stage due to the mixing improvement and better air utilization[27]. In contrast, no NL is registered by the camera. At -0.4 CAD, just after the pilot 2, the flame structure for the hybrid piston is more uniform, burning faster (more intense signal) than for the re-entrant piston. Until this instant, no significant differences can be perceived between both sides of the hybrid piston.

After the main injection, at 10.11 CAD, some dark zones start appearing at the NL images of the re-entrant piston. This is just after the collision between the flames at the bowl's periphery. The absence of natural luminosity in these zones could indicate the existence of cold soot as reported in previous studies [36]. The flame cooling, which could occurs when the flame touches the cold bowl wall, eliminate hot soot sources in these regions. In addition, OH* chemiluminescence measurements present also a signal attenuation in these zones. The OH* attenuation could be linked with the soot presence which avoids the OH* signal to achieve the camera. At the same time, the higher OH* intensity for the hybrid piston evidences a more intense reaction and richer air/fuel ratio regions. This can be related with a better fuel/air mixing process thanks to the flow patterns described previously.

For the hybrid piston, the wave side presents some dark zones too. They are smaller than in the re-entrant case but larger when compared to those observed in the side without waves. Although the flame movement in the wave side is toward the bowl center, the interaction with the colder piston walls could be reducing the flame

temperature and consequently generating soot. The low OH* signal located in the same areas coincides with the dark zones present in the NL images. Furthermore, looking at the squish zone, the stepped lip region of the hybrid piston presents higher OH* intensity than the re-entrant piston. The stepped lip splits the spray into two parts. One of this part, and its kinetic energy, heads toward the squish of the piston promoting air-flow movement in this region and improving the air/fuel mixing. This upper portion of spray impinges on cylinder head and spreads toward the bowl and to the cylinder walls from the squish zone with a significant spreading of mixture and turbulence. This effect enhances the air utilization[37].

At 14.61 CAD, the NL intensity increase indicates that soot oxidation for the three geometries is accelerated. However, it is possible to see that the re-entrant geometry still presents dark zones as discussed previously, which corresponds with low OH* signal too. When this piston is compared with the hybrid one, differences in the OH* intensity are remarkable. This reinforces the idea that soot oxidation is occurring faster for both stepped lip and wave-stepped lip geometries. For the wave side, after the flame starts to move towards the center of the bowl, the rich zones with low OH* signal observable at 10.11 CAD disappear. This increase of the OH* intensity indicates that soot oxidation is accelerated. When comparing between the side with and without wave protrusions, it is possible to see that the waves seems to promote areas close to the bowl center with higher OH* signal intensity than the side without waves.

At 37.7 CAD almost no OH* signal is detected for the hybrid piston while a significant combustion process continues occurring in the re-entrant piston. In this sense, during the so-called late cycle oxidation, both sides of the hybrid piston promote a faster

oxidation than the re-entrant geometry. This agrees with the conclusions extracted from the RoHR analysis[37][18]. Furthermore, the OH* chemiluminesence measurements performed by Eismark et al. [15] reported the faster burn out for the wave piston than for the re-entrant one. The condition of 4.5 bar IMEP presented the same behavior as seen for 7.5 bar IMEP.

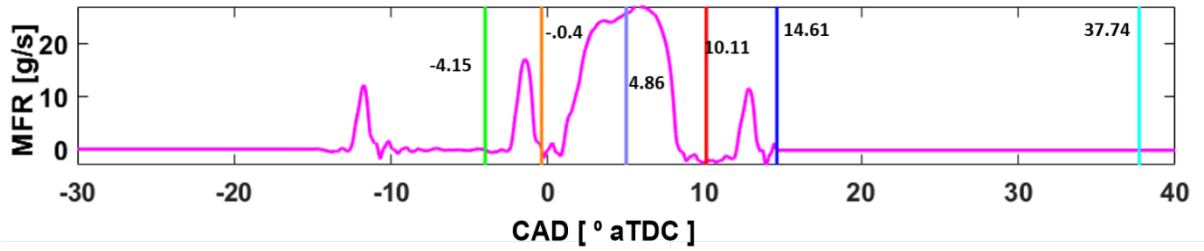

Figure 12- Mass flow rate of the injection at 7.5 bar IMEP

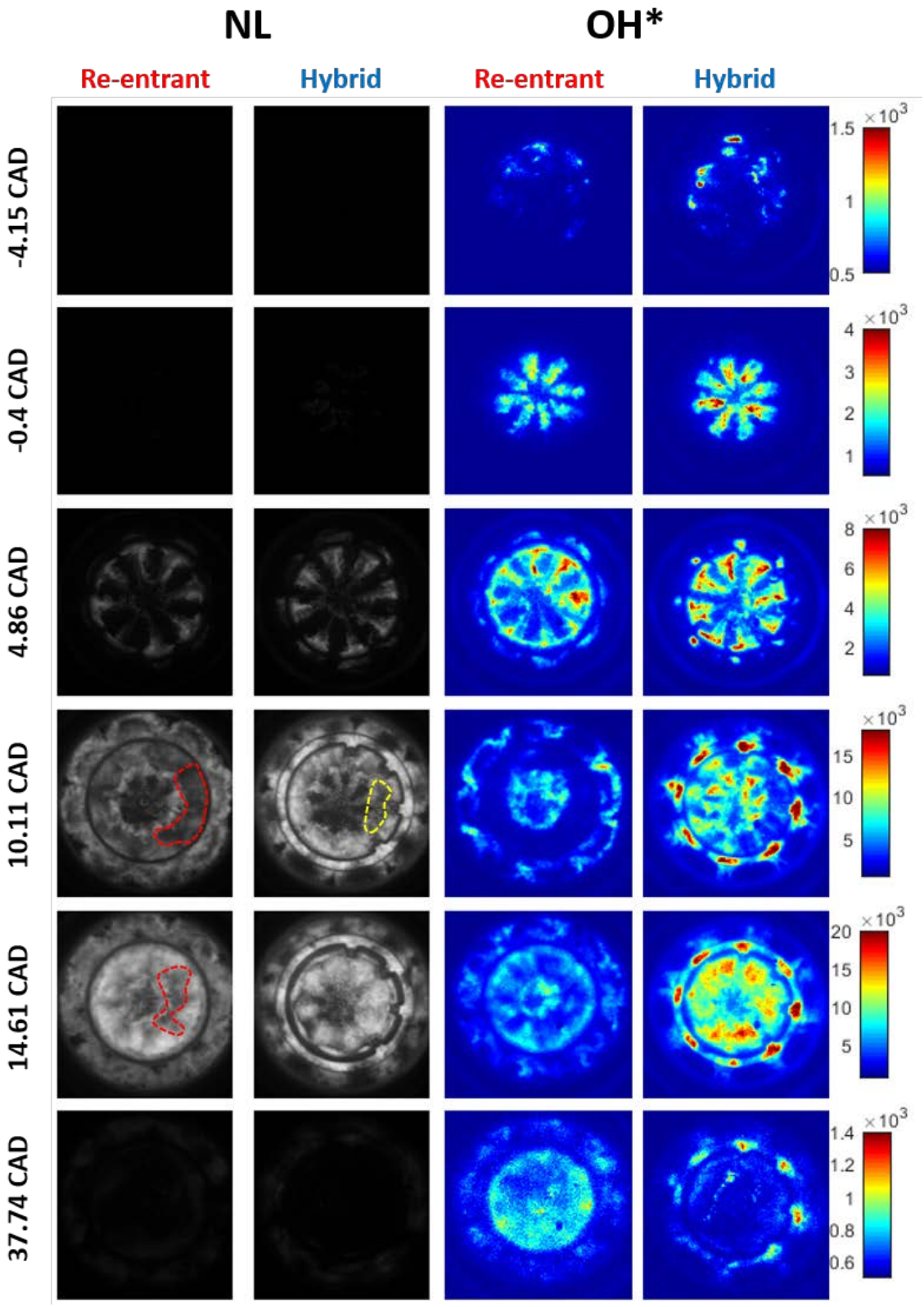

Figure 13- combustion evolution from natural luminosity technique at 7.5 bar IMEP

In order to evaluate the potential of the wave-stepped lip side in comparison with the stepped-lip side and the effect of the reverse flow in the combustion process, an extreme condition in terms of soot generation was also tested by applying a low average air/fuel ratio (λ=1.8) and removing the post injection. The corresponding combustion evolution is presented in figure 14. At this engine condition, the phenomena already presented previously in the reference case were highlighted and new effects could be identified. The effect of reverse flow starts appearing after the spray reaches the bowl wall, where the flame is redirected toward the piston center. At 12.8 CAD, the flame front is closer to the center than in the side without wave protrusions. Eismark et al.[19] reported by using CFD calculations that the wave protrusions are responsible for moving the radial mixing zone, which is located between two adjacent sprays, toward available oxygen in the center of the bowl. A dark U-shaped area, which detaches from the wave protrusion/wall and continues going toward the center, can be observed in the zones highlighted with red lines. This U-shaped area, also reported by Eismark et al. [15], comes from the flame-flame interaction, which occurs later and closer to the bowl center in comparison to the side without waves. In these zones, the oxygen concentration is higher (as they are closer to the center) and the flame-flame collision occurs smoothly, with an incidence angle higher than 0 degrees. It is important to highlight that a portion of hot soot, which is located between the waves and attached to the wall, remains stagnant. In the late combustion cycle, most part of the oxidation process have already occurred, and just specific areas show NL radiation. In this case, the side without wave protrusion seems to present a bigger area with flame in comparison with the side with the waves, indicating that the wave protrusions provide a faster burn out.

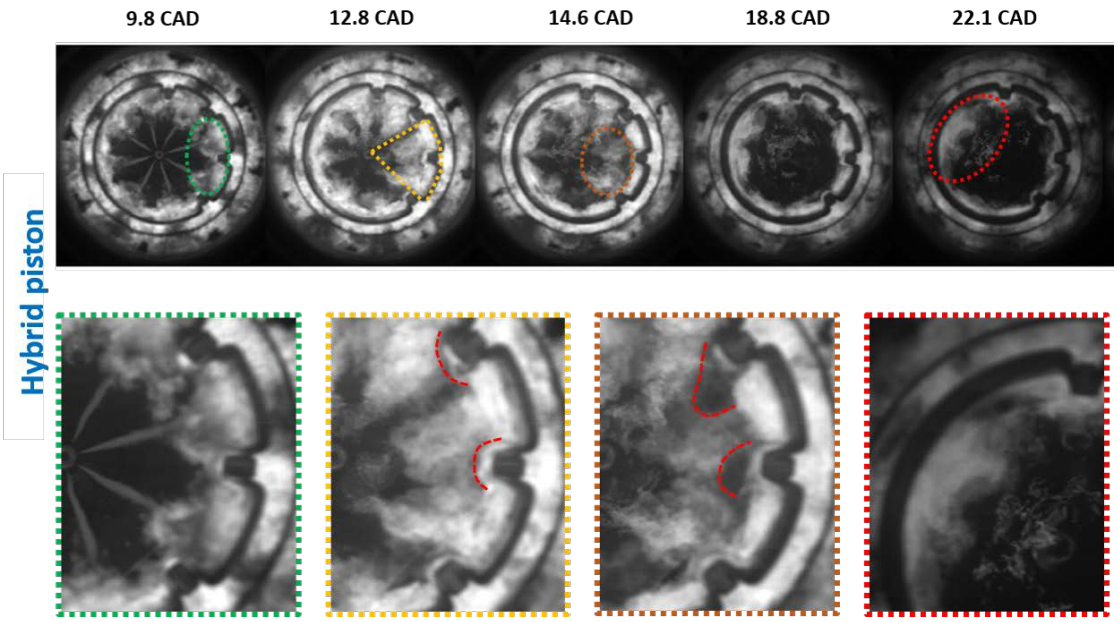

Figure 14. Combustion images of the Wave-Stepped lip piston under extreme conditions of soot generation

4. Conclusions

The present paper has shown an optical study of the effect of different bowl geometries on the combustion process in a compression ignition engine by using different optical techniques. The three techniques, in combination with the in-cylinder pressure analysis, have allowed to identify the differences in terms of flow pattern, flame movement and combustion evolution for each bowl geometry tested. The main results are summarized below:

- The thermodynamic analysis shows that the hybrid piston causes a faster fuel burn, especially visible for the pilot injections, and faster late soot oxidation. However, almost no differences are visible during the main injection and combustion event.
- The wave protrusions induce a reverse flow of the flames towards the bowl center. For the side without waves, the flames seem to stay at the periphery of the bowl contributing to the existence of rich fuel zones. Besides, the flame-

flame collision is smoothed when the flame is driven by this geometry, avoiding frontal collision as it happens in the side without the protrusions and re-entrant piston.

- The velocity field in the re-entrant geometry presents higher velocity values than both sides of the hybrid piston. In the first case, the kinetic energy of the spray is kept inside the bowl. In the second case, spray (and its kinetic energy) is split as in the wave-stepped lip piston. After the main injection have started, the velocities for the re-entrant piston are 20% higher than the wave side of the hybrid piston.
- The wave protrusions direct the flames towards the bowl center, as it is represented by the velocity fields obtained for this geometry. Besides, this effect results in higher velocity values for the wave-stepped lip side than for the side without them. The velocities obtained in the side with waves can be up to 5 m/s higher. Therefore, it can be stated that the wave protrusions compensate the lower kinetic energy inside the bowl when using stepped lip.
- After the post injection, the flow motion inside the re-entrant bowl is governed by the typical swirl movement. The hybrid piston has a different behavior, as velocity values have an increase of 50% due to the post injection effect.
- During the main injection event, re-entrant and wave-stepped lip geometries present similar behavior. In both cases, NL and OH* chemiluminescence signals suggest formation of cold soot after the flame is directed towards the bowl center.
- The wave-stepped lip geometry shows a faster soot oxidation mainly during the late combustion cycle (after post injection). The wave-stepped lip geometry

shows higher OH* signal than the re-entrant geometry at this stage. This indicates the presence of larger near-stoichiometric zones, resulting in a faster soot oxidation. Additionally, OH* signal extinguishes earlier which confirms the end of chemical reactions. When comparing both geometries of the hybrid piston, during late oxidation, the side with waves seems to promote areas close to the bowl center with higher OH* signal intensity than the side without waves.

- Under higher sooting conditions, it was possible to appreciate differences between wave-stepped lip and stepped lip geometries. They appear during the late oxidation process. The waves seem to accelerate the soot oxidation, as it is possible to see that the NL intensity decreases faster than for the side without wave protrusions.

Acknowledgments

The authors gratefully acknowledge General Motors Propulsion Systems-Torino S.r.I. for support the project. Daniel Lérida for his laboratory work on the engine maintenance, operation, and control. This work was partially funded by Generalitat Valenciana through the Programa Santiago Grisolía (GRISOLIAP/2018/142) program.

References

[1] Benajes J, García A, Monsalve-Serrano J, Lago Sari R. Fuel consumption and engine-out emissions estimations of a light-duty engine running in dual-mode RCCI/CDC with different fuels and driving cycles. Energy 2018;157:19–30. https://doi.org/10.1016/j.energy.2018.05.144.

[2] García A, Monsalve-Serrano J, Rückert Roso V, Santos Martins ME. Evaluating the emissions and performance of two dual-mode RCCI combustion strategies under the World Harmonized Vehicle Cycle (WHVC). Energy Convers Manag 2017;149:263–74. https://doi.org/10.1016/j.enconman.2017.07.034.

[3] Benajes J, García A, Monsalve-Serrano J, Balloul I, Pradel G. Evaluating the reactivity controlled compression ignition operating range limits in a high-

compression ratio medium-duty diesel engine fueled with biodiesel and ethanol. Int J Engine Res 2017;18:66–80. https://doi.org/10.1177/1468087416678500.

[4] Benajes J, García A, Monsalve-Serrano J, Boronat V. Dual-fuel combustion for future clean and efficient compression ignition engines. Appl Sci 2017;7. https://doi.org/10.3390/app7010036.

[5] Matamis A, Richter M, Tuner M, Lundgren MO, Andersson O, Arne A, et al. Effects of Post-Injections Strategies on UHC and CO at Gasoline PPC Conditions in a Heavy-Duty Optical Engine. SAE Tech Pap Ser 2017;1. https://doi.org/10.4271/2017-01-0753.

[6] López JJ, García-Oliver JM, García A, Domenech V. Gasoline effects on spray characteristics, mixing and auto-ignition processes in a CI engine under Partially Premixed Combustion conditions. Appl Therm Eng 2014;70:996–1006. https://doi.org/10.1016/j.applthermaleng.2014.06.027.

[7] Kumar S, Dinesha P, Rosen MA. Effect of injection pressure on the combustion, performance and emission characteristics of a biodiesel engine with cerium oxide nanoparticle additive. Energy 2019;185:1163–73. https://doi.org/10.1016/j.energy.2019.07.124.

[8] Pratap B, Goyal R, Deo M, Chaudhary N, Chauhan P. Modelling and experimental study on performance and emission characteristics of citrullus colocynthis (thumba oil) diesel fuelled operated variable compression ratio diesel engine. Energy 2019;182:349–68. https://doi.org/10.1016/j.energy.2019.05.164.

[9] Knothe G. Biodiesel and renewable diesel: A comparison. Prog Energy Combust Sci 2010;36:364–73. https://doi.org/10.1016/j.pecs.2009.11.004.

[10] García A, Monsalve-serrano J, Villalta D, Lago R, Gordillo V, Gaillard P. Potential of e-Fischer Tropsch diesel and oxymethyl-ether (OMEx) as fuels for the dual-mode dual-fuel concept. Appl Energy 2019;253:113622. https://doi.org/10.1016/j.apenergy.2019.113622.

[11] Runge P, Sölch C, Albert J, Wasserscheid P, Zöttl G, Grimm V. Economic comparison of different electric fuels for energy scenarios in 2035. Appl Energy 2019;233–234:1078–93. https://doi.org/10.1016/j.apenergy.2018.10.023.

[12] Liu H, Wang Z, Li Y, Zheng Y, He T, Wang J. Recent progress in the application in compression ignition engines and the synthesis technologies of polyoxymethylene dimethyl ethers. Appl Energy 2019;233–234:599–611. https://doi.org/10.1016/j.apenergy.2018.10.064.

[13] Pastor J V., García A, Micó C, Lewiski F. An optical investigation of Fischer-Tropsch diesel and Oxymethylene dimethyl ether impact on combustion process for CI engines. Appl Energy 2020;260:114238. https://doi.org/10.1016/j.apenergy.2019.114238.

[14] Pastor M, Monsalve-serrano J, Benajes J, García A. Effects of piston bowl geometry on Reactivity Controlled Compression Ignition heat transfer and combustion losses at different engine loads 2016;98:64–77.

https://doi.org/10.1016/j.energy.2016.01.014.

[15] Eismark J, Andersson M, Christensen M, Karlsson A, Denbratt I. Role of Piston Bowl Shape to Enhance Late-Cycle Soot Oxidation in Low-Swirl Diesel Combustion. SAE Int J Engines 2019;12. https://doi.org/10.4271/03-12-03-0017.

[16] Rao L, Zhang Y, Kim D, Su HC, Kook S, Kim KS, et al. Effect of after injections on late cycle soot oxidation in a small-bore diesel engine. Combust Flame 2018;191:513–26. https://doi.org/10.1016/j.combustflame.2018.02.014.

[17] Zha K, Busch S, Warey A, Peterson RC, Kurtz E. A Study of Piston Geometry Effects on Late-Stage Combustion in a Light-Duty Optical Diesel Engine Using Combustion Image Velocimetry. SAE Int J Engines 2018;11:783–804. https://doi.org/10.4271/2018-01-0230.

[18] Busch S, Zha K, Kurtz E, Warey A, Peterson R. Experimental and Numerical Studies of Bowl Geometry Impacts on Thermal Efficiency in a Light-Duty Diesel Engine. SAE Tech Pap Ser 2018;1:1–12. https://doi.org/10.4271/2018-01-0228.

[19] Eismark J, Christensen M, Andersson M, Karlsson A, Denbratt I. Role of fuel properties and piston shape in influencing soot oxidation in heavy-duty low swirl diesel engine combustion. Fuel 2019;254:115568. https://doi.org/10.1016/j.fuel.2019.05.151.

[20] Leach F, Ismail R, Davy M, Weall A, Cooper B. The e ff ect of a stepped lip piston design on performance and emissions from a high-speed diesel engine. Appl Energy 2018;215:679–89. https://doi.org/10.1016/j.apenergy.2018.02.076.

[21] Genzale CL, Reitz RD, Musculus MPB. Effects of piston bowl geometry on mixture development and late-injection low-temperature combustion in a heavy-duty diesel engine. SAE Int J Engines 2009;1:913–37. https://doi.org/10.4271/2008-01-1330.

[22] C. Miles P. The Influence of Swirl on HSDI Diesel Combustion at Moderate Speed and Load. SAE Tech Pap 2000. https://doi.org/10.4271/2000-01-1829.

[23] M. Pickett L, Lopez J. Jet-Wall Interaction Effects on Diesel Combustion and Soot Formation. SAE Tech Pap 2005. https://doi.org/10.4271/2005-01-0921.

[24] Neely GD, Sasaki S, Sono H. Investigation of Alternative Combustion Crossing Stoichiometric Air Fuel Ratio for Clean Diesels. SAE Trans 2007;116:284–94.

[25] Cornwell R, Conicella F. DIRECT INJECTION DIESEL ENGINES. US Patent 8,770,168 B2, 2011.

[26] Smith A. Ricardo low emissions combustion technology helps JCB create the off-highway industry ' s cleanest engine. Ricardo Press Release 2010:4–6.

[27] Dahlstrom J, Andersson O, Tuner M, Persson H. Experimental Comparison of Heat Losses in Stepped-Bowl and Re-Entrant Combustion Chambers in a Light Duty Diesel Engine. SAE Tech Pap 2016. https://doi.org/10.4271/2016-01-0732.

[28] Eismark J, Balthasar M. Device for reducing emissions in a vehicle combustion engine. 8.499,735 B2, 2013.

[29] Dembinski H, Angstrom H-E. Swirl and Injection Pressure Impact on After-Oxidation in Diesel Combustion, Examined with Simultaneous Combustion Image Velocimetry and Two Colour Optical Method. SAE Tech Pap Ser 2013;1. https://doi.org/10.4271/2013-01-0913.

[30] Thielicke W, Stamhuis EJ. PIVlab – Towards User-friendly, Affordable and Accurate Digital Particle Image Velocimetry in MATLAB. J Open Res Softw 2014;2. https://doi.org/10.5334/jors.bl.

[31] Payri F, Molina S, Martín J, Armas O. Influence of measurement errors and estimated parameters on combustion diagnosis. Appl Therm Eng 2006;26:226–36. https://doi.org/10.1016/j.applthermaleng.2005.05.006.

[32] Payri F, Olmeda P, Martín J, García A. A complete 0D thermodynamic predictive model for direct injection diesel engines. Appl Energy 2011;88:4632–41. https://doi.org/10.1016/j.apenergy.2011.06.005.

[33] Pastor J, Olmeda P, Martín J, Lewiski F. Methodology for Optical Engine Characterization by Means of the Combination of Experimental and Modeling Techniques. Appl Sci 2018;8:2571. https://doi.org/10.3390/app8122571.

[34] Dolak JG, Shi Y, Reitz R. A computational investigation of stepped-bowl piston geometry for a light duty engine operating at low load. SAE Tech Pap 2010. https://doi.org/10.4271/2010-01-1263.

[35] Kurtz EM, Styron J. An Assessment of Two Piston Bowl Concepts in a Medium-Duty Diesel Engine. SAE Int J Engines 2012;5:344–52. https://doi.org/10.4271/2012-01-0423.

[36] Roberts G, Lind T, Eagle W, Musculus MP, Andersson Ö, Rousselle C. Mechanisms of Post-Injection Soot-Reduction Revealed by Visible and Diffused Back-Illumination Soot Extinction Imaging. SAE Tech Pap Ser 2018;1:1–20. https://doi.org/10.4271/2018-01-0232.

[37] Busch S, Zha K, Perini F, Reitz R, Kurtz E, Warey A, et al. Bowl Geometry Effects on Turbulent Flow Structure in a Direct Injection Diesel Engine. SAE Tech Pap 2018;2018-Septe. https://doi.org/10.4271/2018-01-1794.

Nomenclature

ICE - Internal combustion engines

CIV- Combustion image velocimetry

IMEP- Indicated mean effective pressure

CI- Compression Ignition

NL- Natural Luminosity

RCCI- Reactivity controlled compression ignition

PPC- Partially premixed combustion

NO_X- Nitrogen dioxide and monoxide

CAD- Crank angle degree

aTDC- After Top Dead Center

CR- Compression Ratio

PM- Particulate Matter

SOE- Start of energizing

SOI- Start of injection

P_{max}- Maximum in-cylinder pressure

FPS- Frames per second

PIV- Particle image velocimetry

HRR- Heat release rate

CA50- Crank angle degree at 50% of total heat release